Performance characterization of tunable longwave infrared notch filters using quantum cascade lasers

Neelam Gupta
Mark S. Mirotznik

Performance characterization of tunable longwave infrared notch filters using quantum cascade lasers

Neelam Gupta[a],* and Mark S. Mirotznik[b]
[a]U.S. Army Research Laboratory, Adelphi, Maryland, United States
[b]University of Delaware, Department of Electrical and Computer Engineering, Newark, Delaware, United States

Abstract. We describe the design and performance characterization of spectrally tunable microengineered notch filters operating in the longwave infrared from 8 to 12 micron using quantum cascade lasers (QCLs) tunable over the full spectral range. The filter design is based on the guided mode resonance phenomenon. The device structure consists of a subwavelength dielectric grating on top of a planar waveguide using high-index transparent dielectric materials, i.e., germanium (Ge) and zinc selenide (ZnSe) with refractive indices of 4.0 and 2.4, respectively. The filters are designed to reflect the incident broadband light at one (or more) narrow spectral band while fully transmitting the rest of the light. Spectral tuning of the reflected wavelength is achieved by changing the angle of incidence by mechanically tilting the filter. Filters based on one-dimensional (1-D) gratings are polarization dependent and those based on two-dimensional (2-D) gratings are close to polarization independent. Simple two-layer antireflection coatings were applied to minimize reflections from the nonpatterned side of the filter substrate. Our experimental setup consisted of a commercial QCL system operating at room temperature, a microengineered filter, and an uncooled broadband sensor. We present the filter design and detailed characterization experiment, and compare the theoretical and experimental results for 1-D filters. © The Authors. Published by SPIE under a Creative Commons Attribution 3.0 Unported License. Distribution or reproduction of this work in whole or in part requires full attribution of the original publication, including its DOI. [DOI: 10.1117/1.OE.57.12.127101]

Keywords: microengineered; subwavelength structures; dielectric grating; planar waveguide; longwave infrared; guided-mode-resonance; spectrally tunable filter; rigorous coupled wave algorithm.

Paper 181359 received Sep. 21, 2018; accepted for publication Nov. 5, 2018; published online Dec. 6, 2018.

1 Introduction

There is a need to develop compact tunable notch or laserline rejection transmission filters operating in the longwave infrared (LWIR) region. Such a filter will efficiently block a single or multiple discrete narrow wavelength band(s), while transmitting light in the rest of the spectral region. Spectrally tunable filters are used for a wide variety of applications in imaging and sensing. Such tunable filters include acousto-optic tunable filters, liquid-crystal tunable filters, Fabry-Perot filters, and so on that operate over many spectral regions including LWIR. Existing spectral filter technologies, however, are inadequate for notch filtering applications as they transmit only a narrow band of light and reject the rest of the light in the spectral region. While filters that can perform notch filtering operation have been developed within the visible to midwave infrared, they are not available in the LWIR region.

In this paper, we present a microengineered metamaterial tunable notch LWIR filter using transparent dielectric materials, germanium (Ge) and zinc selenide (ZnSe) with refractive indices of 4.0 and 2.4, respectively, based on the guided mode resonance (GMR) phenomenon. The resultant filter with subwavelength features possesses a sharp reflectance peak at a designed resonant wavelength while transmitting rest of the light. The resonant wavelength can be tuned mechanically by simply tilting the device with respect to the optical axis. Filters based on one-dimensional (1-D) gratings are polarization-dependent and those based on

two-dimensional (2-D) gratings are close to polarization-independent. We have designed and fabricated prototype notch filters with 1-D gratings and characterized their performance using a room-temperature quantum cascade laser (QCL) system tunable over the full LWIR region from 8 to 12 μm. We present the theoretical background required for modeling and simulation, design of the 1-D filter, the experimental setup, and both the simulation and measurement results and compare them.

2 Guided Mode Resonant Filters

GMRFs are all dielectric filters that exploit the GMR phenomenon. The GMR effect, shown in Figs. 1 and 2, occurs when a transverse guided mode is excited within a dielectric waveguide by the diffracted light from the grating. The resultant-guided modes slowly leak energy due to the index modulation provided by the grating and waveguide combination that interferes with the incident wave producing a filtering response. The excitation of the leaky guided mode will only occur if certain resonant conditions are satisfied. Specifically, the effective index of refraction of the waveguide, n_{wg}, must satisfy

$$\text{Max}[n_{inc}, n_{sub}] \le \left| n_{inc} \sin \theta_{inc} - m \frac{\lambda}{\Lambda_x} \right| < n_{wg}, \tag{1}$$

where n_{inc} and n_{sub} represent the indices of refraction of the incident region and substrate, respectively, θ_{inc} denotes the angle of incidence, λ is the free-space wavelength, m is the diffracted order, and Λ_x is the grating period. When this condition is satisfied, it is possible to design a waveguide and grating structure that results in 100% reflectance over

*Address all correspondence to: Neelam Gupta, E-mail: neelam.gupta.civ@mail.mil
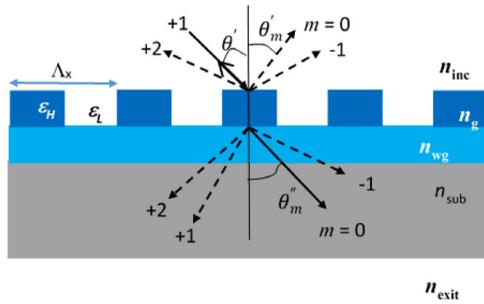
Fig. 1 GMR grating-waveguide layers with diffractive orders illustrated; ε_H and ε_L represent dielectric permittivities for grating and no-grating regions. The refractive indices for each region are labeled.
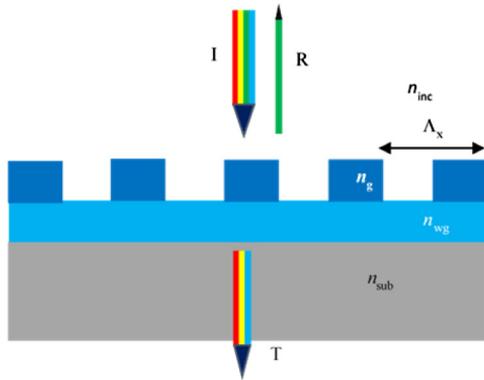
Fig. 2 GMR grating-waveguide layers on a substrate schematically showing reflection at resonant wavelength and transmission at all other wavelengths due to coupling of one diffracted order in waveguide to excite leaky guided mode.

a narrow spectral band. Moreover, as the resonant condition is sensitive to both the geometry of the GMRF stack as well as the angle of incidence, it is feasible to design tunable geometries over a broad spectral band by varying these parameters.[1–9]

3 Basic Filter Configuration

For these devices, we used the filter configuration shown in Fig. 3. Here, the 1-D gratings were fabricated on a Ge waveguide layer deposited on the surface of a thick ZnSe substrate. An antireflective (AR) surface comprising alternating layers of Ge and ZnSe was fabricated on the bottom of the substrate. In the figure, Λ_x is the grating period, h_{wg} is the thickness of the planar waveguide, h_g is the thickness of the grating groove, h_s is the thickness of the substrate, h_{AR1} is the thickness of the Ge layer, and h_{AR2} is the thickness of the ZnSe layer in the AR coating. A rigorous electromagnetic solver was developed to analyze and design the device shown in Fig. 3.

4 Computational Modeling and Design

To predict the wideband electromagnetic properties of the LWIR GMRFs, we chose to implement the rigorous couple wave algorithm (RCWA) originally presented by Moharam and Gaylord.[10,11] Our specific implementation is based on the enhanced transmittance matrix approach introduced
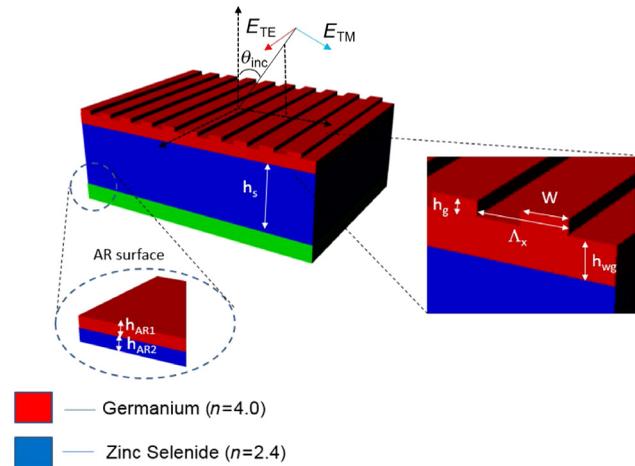
Fig. 3 Basic GMRF configuration for a 1-D device. A grating and a planar waveguide are formed using Ge layers, which are deposited on top of a thick ZnSe substrate. An AR coating, composed of alternating layers of Ge and ZnSe, is deposited on the bottom surface of the substrate. W is the width of grating groove. The direction of incident light and polarization components are also shown.

by Moharam et al.[12] and later refined by Lalanne[4,13] and Noponen and Turunen.[14]

Using this method, the solution domain is divided into discrete infinite planar regions (i.e., incident region, exit region, and layered grating regions) and solved using a modal expansion methodology. For details on the specific implementation of the RCWA, the reader is referred to Refs. 10–14. RCWA simulation results provide a full-wave solution for all reflected and transmitted diffractive orders. However, if the grating periods are small compared with the incident wavelength (λ_o/n_{inc}), as is the case for our GMRF designs, only the zeroth diffractive orders will propagate (i.e., all other diffractive orders will be evanescent). Thus, the filters will reflect and transmit light only in the specular directions. This condition is written mathematically as

$$\Lambda_x < \frac{\lambda_o}{n_{inc}[1 - \sin\theta_{inc}]}. \qquad (2)$$

Our custom RCW code, developed using the MATLAB programming environment, was used to calculate the complex transmission and reflection coefficients for the GMRF designs.

5 Simulation Results

The RCWA method was used to design and simulate a GMRF within the LWIR band from 8 to 12 μm. We used a 1-mm-thick ZnSe substrate with refractive index of 2.41, a Ge waveguide and grating with refractive index equal to 4.0, and a simple two-layer AR coating consisting of Ge and ZnSe layers applied to the bottom of the substrate. The specific geometry of the 1-D GMRF is shown in Fig. 3, and the layer structure and periodic feature used are shown in Table 1. As mentioned, Λ_x is the grating period, W is the width of Ge grating groove equal to the fill factor times the grating period, h_{wg} is the thickness of the planar Ge waveguide, h_g is the thickness of the Ge grating groove, h_s is the thickness of the ZnSe substrate, h_{AR1} is the thickness of

Table 1 Geometrical parameters used for GMRF simulation with 1-D grating structure.

Λ_x (μm)	W (μm)	h_{wg} (μm)	h_g (μm)	h_s (μm)	h_{AR1} (μm)	h_{AR2} (μm)
2.85	1.14	1	0.5	1000	0.3	1.3

the Ge layer, and h_{AR2} is the thickness of the ZnSe layer in the AR coating. Such a filter is polarization-sensitive and to make a polarization-insensitive filter we need to use a 2-D grating. We used the parameters listed in Table 1 to carry out simulations for spectral transmittance of 1-D GMRF for both transverse electric (TE) and transverse magnetic (TM) polarizations of incident light for four different angles of incidence.

In Fig. 4, results are shown for theoretically simulated values of spectral transmittance and reflectance for TE and TM polarizations of the incident light at four different angles of incidence, 0 deg, 9 deg, 15 deg, and 23 deg, respectively. The device parameters were chosen to optimize the filtering operation for the TE polarization when the orientation of the incident light is parallel to the linear grating structure. Several key observations can be made based on these simulated results. The filter is tunable over the full 8- to 12-μm spectral region. A very strong ($\sim$100%) reflectance can be achieved at resonance wavelength using this relatively simple 1-D structure. The line width of such a resonance can be tuned by varying the thickness of the grating. Also, the spectral location of the resonance peak can be tuned by tilting the device (i.e., changing the angle of incidence), which can be done mechanically. However, the single resonance seen at normal incidence splits into two resonances as the device is tilted with respect to the incidence wave. Given the nature of the 1-D grating design, the optical response is polarization sensitive as expected. While both TE and TM polarizations resulted in tunable GMR notch filter responses, the resonance wavelengths are not the same. For less polarization sensitive filters, we are currently exploring the use of 2-D

gratings. Lastly, a high-frequency oscillation is seen in the simulated data due to Fabry–Perot fringing in the thick ZnSe substrate layer. While we did apply an AR coating to the backside of the substrate, the simple nonideal two-layer design we implemented was not very effective. We carried out simulations using multiple layer AR coatings to understand their effect and improve the filter design as discussed next.

As shown in Fig. 5, Fabry–Perot fringing can be markedly reduced by improvements to the AR coating on the backside of the ZnSe substrate. This figure shows that as the number of coating layers is increased, the effectiveness of the AR treatment improves. As discussed above, for our current design used for fabrication, we implemented a simple two-layer AR coating. This was chosen primarily to simplify our fabrication process. However, an optimized eight-layer design would significantly reduce the backside reflections and thus reduce the magnitude of the Fabry–Perot fringes. We should also note that there are other methods that can be employed to reduce the effect of backside reflections including creating a slight wedge to the substrate so that the two surfaces are not parallel. Even a degree or two off parallel will have a large effect on reducing the fringes. We are, currently, exploring these methods experimentally.

6 Performance Characterization Experiment

The prototype filters were fabricated based on the device design shown in Fig. 3 and the specifications listed in Table 1 using standard dielectric deposition and photolithographic techniques and delivered to our laboratory at the US Army Research Laboratory for characterization. A 1-in.-diameter ZnSe substrate polished on both sides with 1-mm thickness was used. The filtering device dimension is 13×13 mm^2. We conducted detailed metrology of the devices using an optical microscope, a scanning electron microscope (SEM), and a profilometer.

Figure 6 shows a photograph of the fabricated device mounted in a holder, an optical microscope image, and a SEM picture for a 1-D filter. The profile of the grating
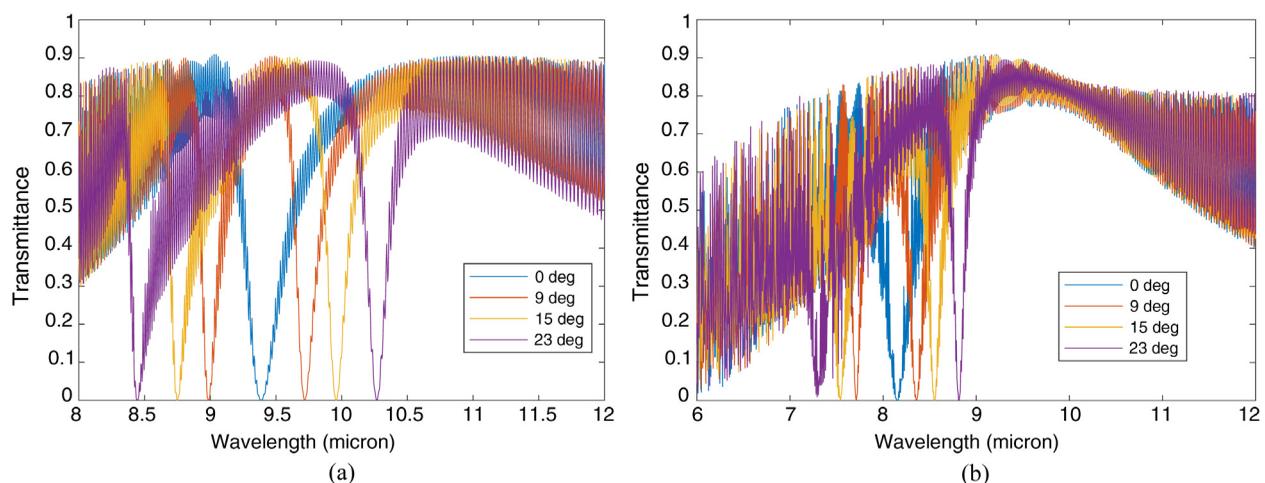
Fig. 4 Simulated spectral transmittance plots using the RCWA method for the device parameters listed in Table 1. (a) Incident polarization is along the grating axis (i.e., TE) and (b) incident polarization is perpendicular to the grating axis (i.e., TM). The four curves are for incidence angles: 0 deg, 9 deg, 15 deg, and 23 deg.
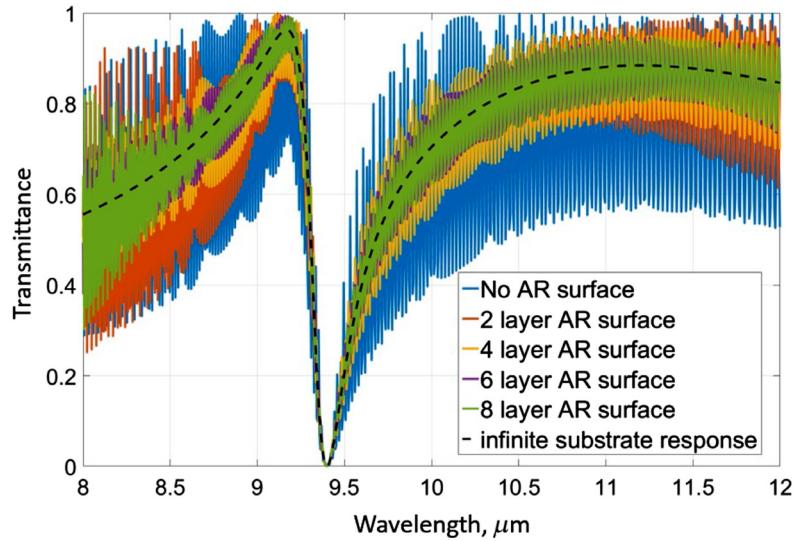
	Ge	ZnSe	Ge	ZnSe	Ge	ZnSe	Ge	ZnSe
No AR	NA	NA	NA	NA	NA	NA	NA	NA
2 layer AR	0.3μm	1.3μm	NA	NA	NA	NA	NA	NA
4 layer AR	0.21μm	0.30μm	0.68μm	1.01μm	NA	NA	NA	NA
6 layer AR	0.15μm	0.40μm	2.49μm	2.03μm	0.58μm	1.03μm	NA	NA
8 layer AR	0.21μm	0.29μm	0.62μm	0.1μm	0.19μm	2.0μm	0.57μm	1.05μm

Fig. 5 To minimize the Fabry–Perot fringing effect more sophisticated AR surface designs can be implemented. The top plot shows simulation results of how increasing the number of AR coatings layers from two layers (our current design) to eight layers significantly reduces back reflections from the thick ZnSe substrate and thus a large reduction in the magnitude of the Fabry–Perot fringes. Also shown in the figure (black dashed line) is the ideal filter response if the substrate was infinitely thick (i.e., no back reflections). A table is included listing the number of Ge and ZnSe layers and thicknesses used in the simulations.

(a) (b) (c)
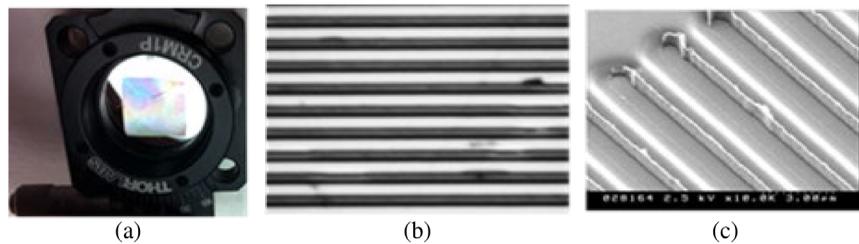
Fig. 6 (a–c) Photo of 13- × 13-mm^2 filter, optical microscope picture of a fabricated device, and an SEM image.

was measured using a Veeco profilometer. The profilometer measured the grating period to be 2.85 μm for a 1-D GMRF.

Traditionally, a Fourier transform infrared (FTIR) spectrometer is used to measure filter transmission. The FTIR spectrometer in our laboratory operates with incident beam focused on the sample and to obtain a collimated beam as required for plane wave incidence needs a major upgrade. Instead of using this FTIR spectrometer, we chose to use a QCL system that is tunable over the full range of filter operation to carry out direct transmission measurements. In Fig. 7, we show a photograph of the experimental setup to characterize the performance of fabricated filters using
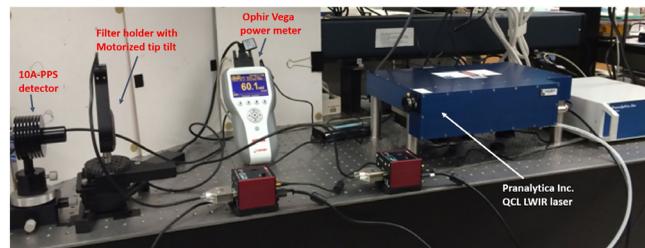
Fig. 7 Experimental setup consisting of QCL tunable LWIR laser, Ophir–Spiricon pyrocam detector, rotating stage to hold filter sample and custom Labview interface for automated filter characterization.

a QCL system and a thermal detector. The details of the setup are described in following three subsections.

6.1 Tunable Laser Source

We used a QCL system that can be tuned in the spectral range from 8.2 to 12.0 μm to characterize the transmission of the filters. In Table 2, we list the salient characteristics of an air-cooled, computer-controlled quasicontinuous wave (QCW) QCL system (Pranalytica Inc. model OmniLux-80-90-100-110). We used three laser diodes in this system as shown in Table 2. Each laser diode is single mode with very small sidelobes (<3% peak power as compared to main lobe). Figure 8 shows the measured QCL power spectrum and a typical beam profile of the QCLs as measured by an Ophir–Spiricon Pyrocam IV camera. A collimated TE-polarized incident laser beam that covers overall filter area was used to be consistent with the incident plane wave assumption made in the theory.

6.2 Detector

An Ophir–Spiricon model Vega-B power meter with a 10A-PPS uncooled broadband thermopile detector with a 16-mm aperture was used to measure the intensity of light transmitted by the filter. The operation of the power meter is computer controlled.

6.3 Filter Holder

The filter was mounted using two computer-controlled rotational stages. It can be rotated about an axis perpendicular to

the filter plane to preciously line up the grating groove direction with the polarization of the incident light. The filter can also be rotated about a vertical axis parallel to the filter plane to adjust the angle of incidence.

7 Performance Characterization Results

In Fig. 9, the measured transmittance spectra with TE-polarized laser light for a prototype filter with 1-D grating for four angles of incidence 0 deg, 9 deg, 15 deg, and 23 deg are shown, respectively. The graph shown here is acquired by measuring the average transmitted laser intensity at each wavelength for various filter tilt angles. Note that the high-frequency oscillations predicted by the RCW simulations are present in the measured data. Improved AR surface treatments will reduce these effects. As mentioned in Sec. 5, there is only one resonance notch for the normal incidence of light and there are two separate notches for non-normal incidence. In Table 3, we compare the values of resonant wavelengths obtained from both the computer simulation and experimental measurement. It is clear from this table that experimental values are close to the simulated ones considering the experimental error. We also observed in the measured data, however, reduced transmission at the longer wavelength (>10.5 μm) that is not predicted by simulations. We are currently exploring the reasons for this lower than expected transmission, but currently suspect it is greater than expected material loss at the longer wavelengths that are not accounted for in the model.

Table 2 Salient characteristics of QCL system.

Laser	Spectral range (μm)	Pulse frequency (MHz)	Peak wavelength (μm)	Measured peak power (mW)	Beam diameter at 1 m in mm	Output beam
QCL 1	8.20 to 9.59	1.0	8.6	81	5.2 (major) 4.4 (minor	Collimated
QCL 2	9.60 to 10.70	1.0	9.9	88	5.1 (major) 4.4 (minor)	Collimated
QCL 3	10.71 to 12.50	1.0	11.5	29.3	6.2 (major) 4.1 (minor)	Collimated
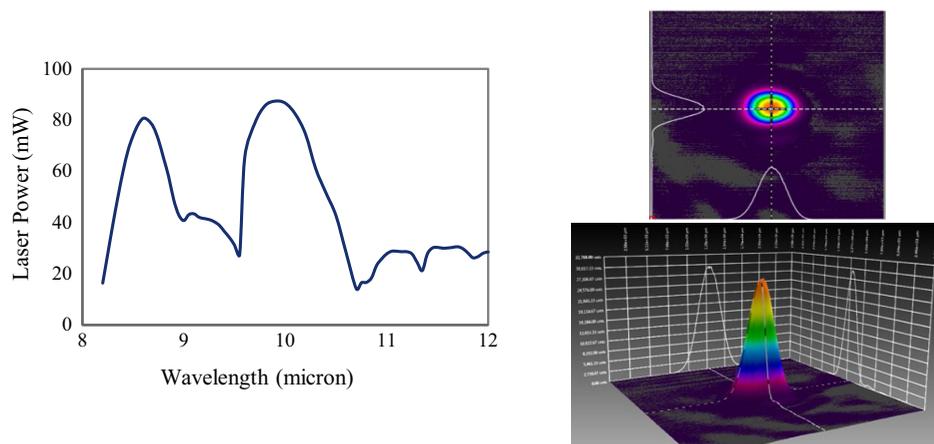
Fig. 8 Measured laser power and a typical beam profile of a QCL.
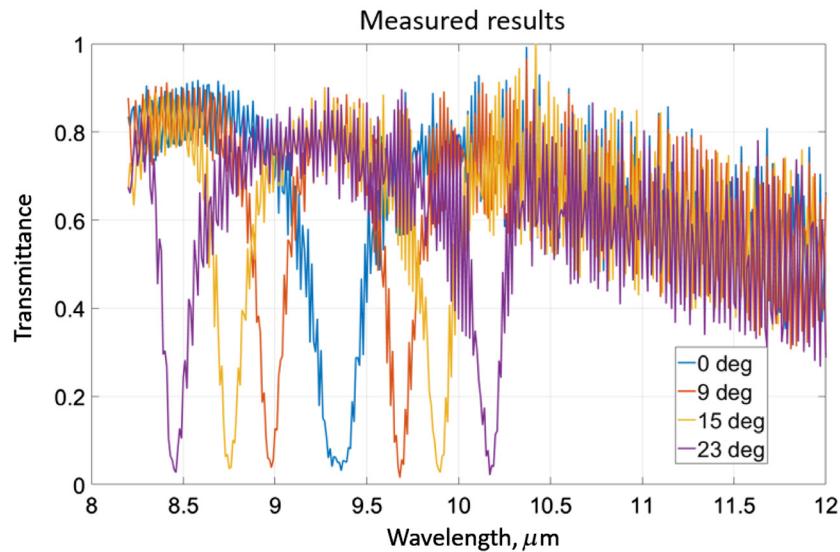
Fig. 9 Measured 1-D GMRF transmission spectra for TE-polarized light at four incidence angles: 0 deg, 9 deg, 15 deg, and 23 deg.

Table 3 Simulation and experimental values of resonance wavelengths for 1-D GMRF.

Angle of incidence (deg)	Resonance wavelengths for TE polarization (μm)	
	Simulation	Experiment
0	9.38	9.36
9	8.98, 9.72	8.98, 9.68
15	8.75, 9.95	8.75, 9.9
23	8.44, 10.26	8.46, 10.17

8 Discussion and Conclusion

We designed spectrally tunable notch filters using the GMR phenomenon in a microengineered device with a subwavelength periodic Ge grating structure on a Ge planar waveguide deposited on a ZnSe substrate. Filters with 1-D gratings were designed to operate in 8- to 12-μm spectral region. As the notch filters with 1-D grating feature are sensitive to the incident polarization, we designed such filters for the TE-polarized light. Prototype filters were fabricated using standard dielectric deposition and photolithographic techniques. Such filters can be spectrally tuned by changing the angle of incidence by mechanically tilting the filter about the optical axis. We characterized prototype filters using a commercial room-temperature QCL system tunable over the 8- to 12-μm spectral region. Our experimental results match closely with the theoretical predictions. High-frequency oscillations in both the experimental and theoretical data were observed due to multiple reflections in the 1-mm-thick ZnSe substrate. The contribution from low QCL sidelobes to the noise is extremely small. The traditional method of characterizing spectral filters uses a Fourier transform infrared spectrometer (FTIR), which could not be used for our filters, as a collimated incident beam of light is needed to illuminate the filter, and is not available in a typical FTIR.

We used a simple two-layer AR coating on the backside of the substrate, which while not overly effective at reducing the high-frequency noise can be improved. We plan to improve the AR coating design using optimization techniques and are looking into using multiple layers and a wedged substrate. We are carrying out additional investigations to understand transmission losses due to the spectral dependence of the materials used.

We also plan on improving the filter fabrication process to improve the filter performance. We are upgrading a Bruker Vertex 70 FTIR to be able to take measurements with a normal incidence of light. This will facilitate rapid characterization of filters during and after fabrication process. We also plan to fabricate and characterize 2-D GMRFs to understand their spectral and polarization dependence in detail.

References

1. S. S. Wang and R. Magnusson, "Theory and applications of guided-mode resonance filters," *Appl. Opt.* **32**, 2606–2613 (1993).
2. R. Magnusson and Y. Ding, "MEMS tunable resonant leaky mode filters," *IEEE Photonics Technol. Lett.* **18**, 1479–1481 (2006).
3. R. Magnusson and M. Shokooh-Saremi, "Widely tunable guided-mode resonance nanoelectromechanical RGB pixels," *Opt. Express* **15**(17), 10903–10910 (2007).
4. P. Lalanne and J. Hugonin, "High-order effective-medium theory of subwavelength gratings in classical mounting: application to volume holograms," *J. Opt. Soc. Am. A* **15**, 1843–1851 (1998).
5. N. Gupta and M. S. Mirotznik, "Characterization of tunable longwave infrared filters using quantum cascade lasers," *Proc. SPIE* **10541**, 105411B (2018).
6. M. S. Mirotznik et al., "Long wave Infrared tunable filter based on guided mode resonant effect," *Proc. SPIE* **9855**, 98550L (2016).
7. Y. H. Ko and R. Magnusson, "Zero-contrast silicon-based metasurfaces: resonance physics and applications," *Proc. SPIE* **10356**, 103560N (2017).
8. Y. Zhong et al., "Mid-wave infrared narrow bandwidth guided mode resonance notch filter," *Opt. Lett.* **42**, 223–226 (2017).
9. J.-N. Liu et al., "Optimally designed narrowband guided-mode resonance reflectance filters for mid-infrared spectroscopy," *Opt. Express* **19**, 24182–24197 (2011).
10. M. G. Moharam and T. K. Gaylord, "Rigorous coupled-wave analysis of planar-grating diffraction," *J. Opt. Soc. Am. A* **71**, 811–818 (1981).

11. M. G. Moharam et al., "Formulation for stable and efficient implementation of the rigorous coupled wave analysis of binary gratings," *J. Opt. Soc. Am. A* **12**, 1068–1076 (1995).
12. M. G. Moharam, D. A. Pommet, and E. B. Grann, "Stable implementation of the rigorous coupled-wave analysis for surface relief gratings: enhanced transmittance matrix approach," *J. Opt. Soc. Am. A* **12**, 1077–1086 (1995).
13. P. Lalanne, "Improved formulation of the coupled-wave method for two-dimensional gratings," *J. Opt. Soc. Am. A* **14**, 1592–1598 (1997).
14. E. Noponen and J. Turunen, "Eigenmode method for electromagnetic synthesis of diffractive element with three-dimensional profiles," *J. Opt. Soc. Am. A* **11**, 2494–2502 (1994).

Neelam Gupta is a research physicist in the Sensors and Electron Devices Directorate of the Army Research Laboratory, Adelphi, Maryland. She has a PhD in physics. She developed a number of compact multispectral/hyperspectral imagers from the ultraviolet to the longwave infrared using acousto-optic tunable filters, diffractive optics, MEMS based filters, etc. Currently, she is working on the development of tunable optical notch filters. She is a senior member of the Optical Society of America.

Mark S. Mirotznik received his BSEE degree from Bradley University, Peoria, Illinois, in 1988 and his MSEE and PhD degrees from the University of Pennsylvania, Philadelphia, in 1991 and 1992, respectively. Currently, he is a professor in the Department of Electrical and Computer Engineering at the University of Delaware, in Newark, Delaware. His research interests include applied electromagnetics and photonics, computational electromagnetics, multifunctional engineered materials and additive manufacturing.